ELSEVIER

Catalysis Today 37 (1997) 309–329

CATALYSIS TODAY

The role of coke formation in catalytic partial oxidation for synthesis gas production

Ann M. De Groote*, Gilbert F. Froment

Universiteit Gent, Laboratorium voor Petrochemische Techniek, Krijgslaan 281, B-9000 Gent, Belgium

Abstract

The partial oxidation of CH_4/O_2- and CH_4/air-mixtures into synthesis gas on a $Ni/MgO/Al_2O_3$-catalyst in an adiabatic fixed bed reactor was modelled. Diffusional limitations on the various reactions were accounted for through effectiveness factors, averaged over the operating conditions and calculated from a number of off line pellet simulations. The evolution of the coke content of the catalyst with time was included in the simulation so as to check whether or not a steady state reactor operation was possible. The influence of the feed composition (addition of steam and carbon dioxide) and the operating conditions on the coke content was also investigated. For constant methane flow rate and constant total pressure the partial pressure of oxygen decreases when steam is added. This leads to a higher coke content of the catalyst, while coke deposition occurs in a larger area of the reactor, since oxygen is a stronger oxidant than steam.

Keywords: Catalytic partial oxidation; Methane conversion; Syngas production

1. Introduction

The increasing natural gas production led to a growing interest in its conversion into various types of synthesis gas for processes like Fischer–Tropsch synthesis, methanol synthesis, oxo-synthesis, etc.

So far, natural gas is converted to syngas mainly by means of steam reforming, CO_2-reforming and non-catalytic partial oxidation. An alternative process for syngas production is the catalytic partial oxidation of natural gas with air or oxygen.

In this process the highly exothermic combustion of a fraction of the natural gas feed

$$CH_4 + 2O_2 \rightarrow CO_2 + 2H_2O \quad (1)$$

provides the heat and the reactants for the endothermic steam reforming

$$CH_4 + H_2O \rightleftharpoons CO + 3H_2 \quad (2)$$

and the endothermic CO_2-reforming

$$CH_4 + CO_2 \rightleftharpoons 2CO + 2H_2 \quad (3)$$

*Corresponding author.

PII S0920-5861(97)00013-8

of the remaining methane (the main component of natural gas). The above reactions are of course accompanied by the water gas shift reaction

$$CO + H_2O \rightleftharpoons CO_2 + H_2 \quad (4)$$

In the partial oxidation of methane, carbon can be deposited to various degrees according to the endothermic methane cracking

$$CH_4 \rightleftharpoons C + 2H_2 \quad (5)$$

and the slightly exothermic Boudouard reaction or CO-disproportionation

$$2CO \rightleftharpoons C + CO_2 \quad (6)$$

The coke can be removed by steam gasification

$$C + H_2O \rightleftharpoons CO + H_2 \quad (7)$$

or burnt off with oxygen

$$C + O_2 \rightleftharpoons CO_2 \quad (8)$$

Coking inside the catalyst pores can lead to deactivation and even complete disintegration of the catalyst particle. Therefore, it is important to control or avoid carbon deposition by using appropriate feed conditions and operating conditions. Coke deposition can also be reduced by catalyst additives. A small amount of magnesia is effective, though care should be taken, since hydration of MgO weakens the catalyst [1].

The present paper deals with the simulation of coke deposition in the catalytic partial oxidation of methane into synthesis gas with air or oxygen on a $Ni/MgO/Al_2O_3$-catalyst in an adiabatic unidirectional fixed bed reactor.

2. Modelling of the unidirectional fixed bed reactor

2.1. Rate equations

According to Prettre et al. [2] and Vernon et al. [3] partial oxidation of methane is a combination of reactions (1)-(4). This set of reactions is equivalent to the set formed by the total combustion reaction (1) and three reactions representative of steam reforming:

$$CH_4 + H_2O \rightleftharpoons CO + 3H_2 \quad (2)$$

$$CH_4 + 2H_2O \rightleftharpoons CO_2 + 4H_2 \quad (3a)$$

$$CO + H_2O \rightleftharpoons CO_2 + H_2 \quad (4)$$

Indeed, reaction (3) is a linear combination of reactions (3a) and (4).

For the modelling of the catalytic partial oxidation of methane this set of reactions ((1), (2), (3a) and (4)) is combined with the carbon formation and gasification reactions (5)–(8). Kinetic equations have been reported in the literature for each of these reactions. An overview of the published rate equations for the total combustion reaction is given by Cullis et al. [4]. Most of these rate equations were derived under conditions with excess oxygen, however, thus leading to a zero-order dependence on the partial pressure of oxygen, while in the partial oxidation process substoichiometric CH_4/O_2-feed ratios are applied. Trimm and Lam [5] have developed a rate equation for the total combustion of methane into CO_2 and H_2O under oxygen deficient conditions ($0.33<CH_4/O_2<2$) and at high temperature, but unfortunately on a Pt-catalyst, not on a Ni-catalyst. In the absence of kinetic equations for the total combustion reaction on a Ni-catalyst for operating conditions similar to those of the partial oxidation of natural gas, the expression of Trimm and Lam [5] is implemented in the simulation model of the present paper. Assuming that the rate determining step is the surface reaction between adsorbed methane on the one hand and both diatomically

adsorbed oxygen or gaseous oxygen on the other hand, they obtained the following rate equation:

$$r_1 = \frac{k_1 p_{CH_4} p_{O_2}}{(1 + K_1 p_{CH_4} + K_2 p_{O_2})^2} + \frac{k_2 p_{CH_4} p_{O_2}^{1/2}}{1 + K_1 p_{CH_4} + K_2 p_{O_2}}.$$

For the steam reforming reactions the kinetic model of Xu and Froment [6] is applied. This model is known to be one of the most general ones, accounting for the non-monotonic dependence of the reaction rate upon the partial pressure of steam and accurately predicting industrial values (Soliman et al. [7]). The corresponding rate equation for CO-production by steam reforming (reaction (2)) is

$$r_2 = \frac{(k_3/p_{H_2}^{2.5})(p_{CH_4} p_{H_2O} - (p_{H_2}^3 p_{CO}/K_3))}{(1 + K_{CO} p_{CO} + K_{H_2} p_{H_2} + K_{CH_4} p_{CH_4} + K_{H_2O}(p_{H_2O}/p_{H_2}))^2}.$$

The rate of CO_2-production by steam reforming (reaction (3a)) can be calculated according to

$$r_3 = \frac{(k_4/p_{H_2}^{3.5})(p_{CH_4} p_{H_2O}^2 - (p_{H_2}^4 p_{CO_2}/K_4))}{(1 + K_{CO} p_{CO} + K_{H_2} p_{H_2} + K_{CH_4} p_{CH_4} + K_{H_2O}(p_{H_2O}/p_{H_2}))^2},$$

while the rate of the water gas shift reaction is given by

$$r_4 = \frac{(k_5/p_{H_2})(p_{CO} p_{H_2O} - (p_{H_2} p_{CO_2}/K_5))}{(1 + K_{CO} p_{CO} + K_{H_2} p_{H_2} + K_{CH_4} p_{CH_4} + K_{H_2O}(p_{H_2O}/p_{H_2}))^2}.$$

A problem encountered in the partial oxidation of methane on Ni/Al_2O_3 is the degree of reduction of the catalyst. For steam reforming to occur the Ni-catalyst should be in the reduced state. Yet, in the presence of oxygen the catalyst is oxidised. According to Dissanayake et al. [8], the Ni-catalyst can exhibit three different reduction states in the partial oxidation of methane. In the presence of oxygen and at temperatures below 700°C the catalyst is in the form of $NiAl_2O_4$ and shows a moderate activity for the total combustion reaction. Above 700°C $NiAl_2O_4$ decomposes into Al_2O_3 and NiO, with a high activity for the combustion into CO_2 and H_2O. Finally a reduced Ni-phase is formed and the reforming reactions take off.

In order to account for this varying degree of reduction of the catalyst in what will be called the VDR-model, the rates of the reforming reactions (2), (3a) and (4) are multiplied by the catalyst reduction factor, $(x_{O_2})^{12}$, a power function of the fractional conversion of oxygen. By means of this reduction factor, the reforming reactions are gradually growing in importance as oxygen is consumed by reaction (1).

A comprehensive kinetic study of methane cracking, the Boudouard reaction and carbon gasification by hydrogen, steam and carbon dioxide has been performed by Wagner and Froment [9] and by Snoeck and Froment [10]. In previous work [11,12] the kinetics developed by Wagner and Froment [9] were applied in the simulation of the steady state partial oxidation of methane into synthesis gas. In the present work the rate equations of Snoeck and Froment [10] are built into the simulation model.

In previous work [11,12] the rate equation for carbon gasification with oxygen was independent of the amount of coke deposited on the catalyst surface. In the present work, the rate equation of Weisz and Goodwin [13] is used. This is an empirical rate equation for carbon gasification by oxygen under reaction conditions similar to those of partial oxidation. Since carbon gasification by oxygen is a gas–solid reaction, the concentration of the carbon has to enter into the rate equation to account for the transport through a more or less porous structure of the solid. Coke gasification can occur uniformly or shell-progressively. In the latter case, the reaction occurs in a narrow shell of the catalyst pellet, that moves progressively from the boundary to the centre of the pellet. Based upon a combination of several transport and diffusion phenomena Weisz and Goodwin [13] obtained a rate equation for carbon gasification by oxygen of the form:

$$r_8 = k n_C p_{O_2}$$

with n_C the amount of coke deposited on the catalyst surface.

The application of this rate equation in the reactor simulation program implies an additional continuity equation for carbon.

2.2. Reactor model

In the simulation of the catalytic partial oxidation of natural gas into synthesis gas in a unidirectional fixed bed reactor, a one-dimensional heterogeneous model is applied [14]. Temperature and concentration gradients are accounted for in axial direction only. The gradients over the fluid film surrounding the catalyst pellet are negligible because of the high superficial gas velocity associated with the Reynolds number based upon the particle diameter, which is of the order of 200.

Since severe diffusional limitations are encountered in steam reforming [15], it can be expected that this will be the case in partial oxidation too. Diffusional limitations inside the catalyst pellet are accounted for in the reactor model by means of averaged effectiveness factors, based upon a number of off-line pellet simulations. The values of the effectiveness factors for the various reactions are:

- for the total combustion of CH_4 into CO_2 and H_2O: η_1=0.05,
- for CO-production by steam reforming: η_2=0.07,
- for CO_2-production by steam reforming: η_3=0.06,
- for the WGS-reaction: η_4=0.7.

The four main reactions are diffusion limited and lead to concentration gradients inside the catalyst pellets. This also affects the rates of the coking and gasification reactions and is accounted for by means of the effectiveness factors:

- for methane cracking: η_5=0.05,
- for the Boudouard reaction: η_6=0.05,
- for C-gasification by steam: η_7=0.05,
- for C-gasification by oxygen: η_8=0.05.

The reactor model consists of the following set of ordinary differential equations:
The continuity equations for the various components are

$$\frac{dx_{CH_4}}{dz} = \frac{\rho_b \Omega}{F^0_{CH_4}}(\eta_1 r_1 + \eta_2 r_2 + \eta_{3a} r_{3a} + \eta_5 r_5),$$

$$\frac{dx_{O_2}}{dz} = \frac{\rho_b \Omega}{F^0_{O_2}}(2\eta_1 r_1 + \eta_8 r_8),$$

$$\frac{dx_{CO}}{dz} = \frac{\rho_b \Omega}{F^0_{CH_4}}(\eta_2 r_2 - \eta_4 r_4 - 2\eta_6 r_6 + \eta_7 r_7),$$

$$\frac{dx_{CO_2}}{dz} = \frac{\rho_b \Omega}{F^0_{CH_4}}(\eta_1 r_1 + \eta_{3a} r_{3a} + \eta_4 r_4 + \eta_6 r_6 + \eta_8 r_8),$$

$$\frac{dC_C}{dt} = r_C.$$

The energy equation is

$$\frac{dT}{dz} = \frac{\rho_b}{u_s \rho_g c_p} \sum_{i=1}^{8} \eta_i r_i (-\Delta H)_i.$$

The pressure drop equation is

$$\frac{dp_t}{dz} = -\frac{f\rho_g u_s^2}{d_p}.$$

Since no deactivation functions are available for the partial oxidation process, deactivation by carbon deposition is not accounted for in the simulations.

2.3. Numerical solution

The integration of the first-order differential equations in axial direction was performed by means of a fifth-order Runge–Kutta routine with variable step size [16]. It was superimposed on the time integration of the continuity equation for coke.

3. Simulation results and discussion

3.1. Simulation of an industrial adiabatic unidirectional fixed bed reactor for the partial oxidation with air

A simulation of the partial oxidation of methane with air in an industrial reactor with a length of 6 m and an internal diameter of 1.2 m, was performed for the operating conditions given in Table 1. The time evolution of the coke content through the reactor is given in Fig. 1. The zone of the reactor where carbon is deposited decreases with time, while the coke content of the catalyst at the reactor outlet increases. After some time a steady state reactor operation is established, as will be illustrated below.

The temperature profiles through the catalyst bed after various times of reactor operation are given in Fig. 2. It is clear from this figure that the reaction front moves towards the reactor inlet as time increases, while the exit temperature decreases. Furthermore, two humps are observed in the temperature profiles.

The displacement of the reaction front towards the inlet of the catalyst bed can be explained in terms of the evolution of the rate of carbon gasification by oxygen, shown in Fig. 3. Carbon gasification by oxygen is a very exothermic reaction and leads to a temperature profile in the first part of the bed which becomes steeper with time. The rates of the other reactions increase, so that the reaction zone moves towards the reactor inlet.

The observed phenomena will be discussed in detail based upon Fig. 4, where the evolution of the net coking rate, consisting of coke formation and gasification is shown in the first part of the reactor after 5 min of operation. The rate of carbon gasification by steam is not shown since it is negligible. It follows from Fig. 4 that the reactor can be divided into four zones. In zone I, the net coking rate decreases and from a certain axial position onwards gasification occurs. The gasification rate increases and reaches a maximum, while it decreases again in zone II. In zone III carbon gasification becomes more important and eventually carbon free operation becomes possible in zone IV, which extends to the end of the reactor.

Table 1
Feed conditions and reactor dimensions

Inlet pressure, p_t^0	25 atm
Inlet temperature, T^0	808 K
Total inlet flow rate, F_t^0	18 375 Nm^3/h
H_2O/CH_4-feed ratio	1.4
CH_4/O_2-feed ratio	1.6722
Inlet mole fraction of H_2, $y_{H_2}^0$	0.0001
Inlet mole fraction of CO_2, $y_{CO_2}^0$	0
Reactor length, L	6 m
Reactor diameter, D_i	1.2 m

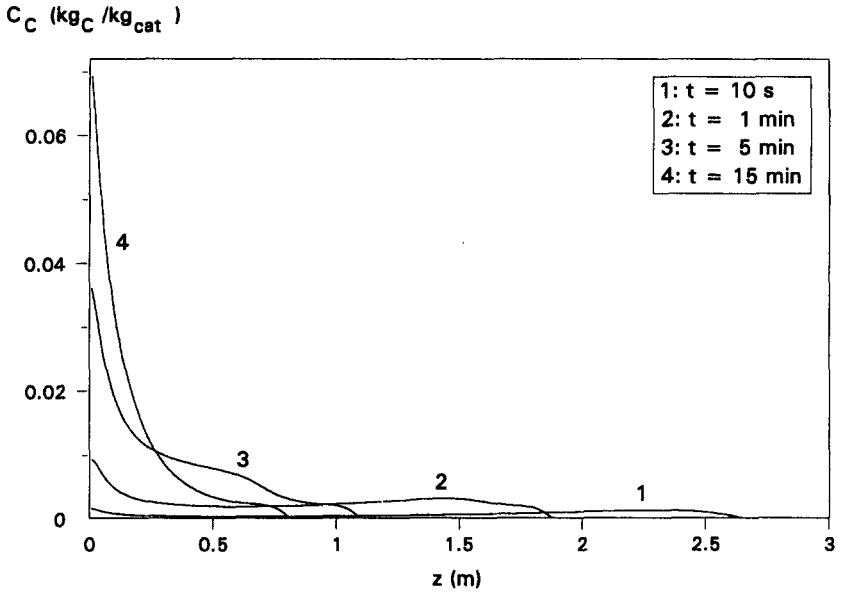

Fig. 1. Coke content of the catalyst through the reactor for several run lengths.

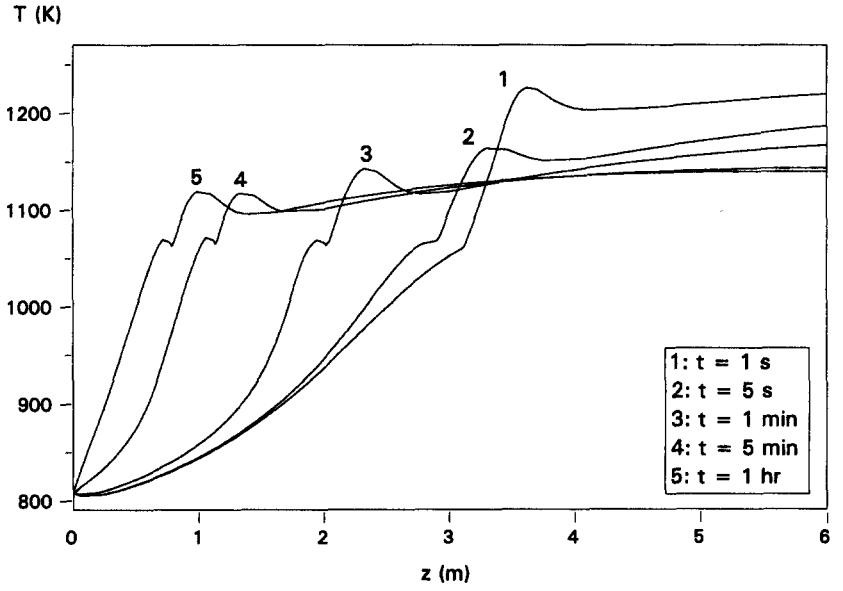

Fig. 2. Temperature profile through the catalyst bed for several run lengths.

In zone I, the rate of methane cracking does not increase as much as would be expected from the temperature rise, because of the decreasing partial pressure of methane and the increasing partial pressure of hydrogen. The reverse Boudouard reaction becomes faster, since more carbon dioxide is produced further downstream in the reactor, due to the total combustion of methane and the oxygen gasification of the coke. Furthermore, the rate of carbon gasification by oxygen progressively increases, leading to a decrease in the net coking rate and eventually leading to gasification.

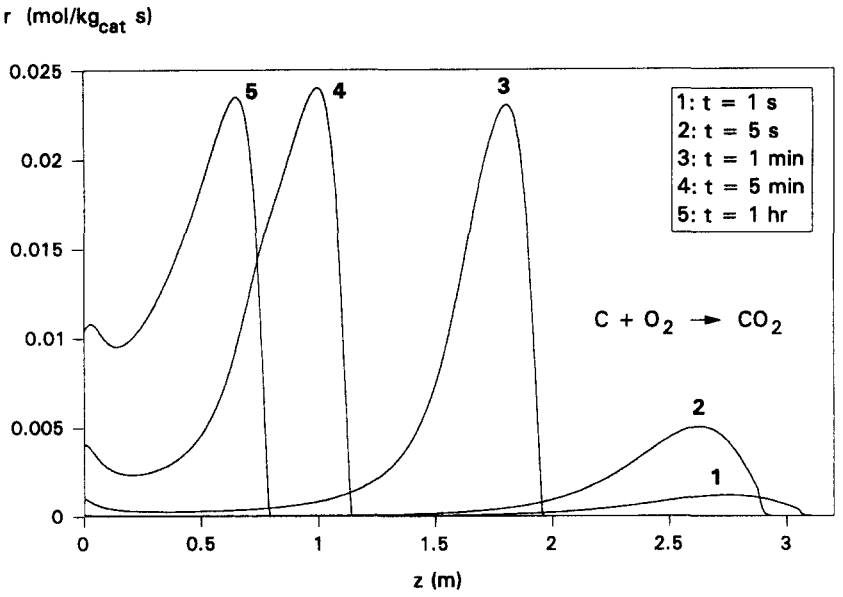

Fig. 3. Rate of carbon gasification by oxygen through the catalyst bed for several run lengths.

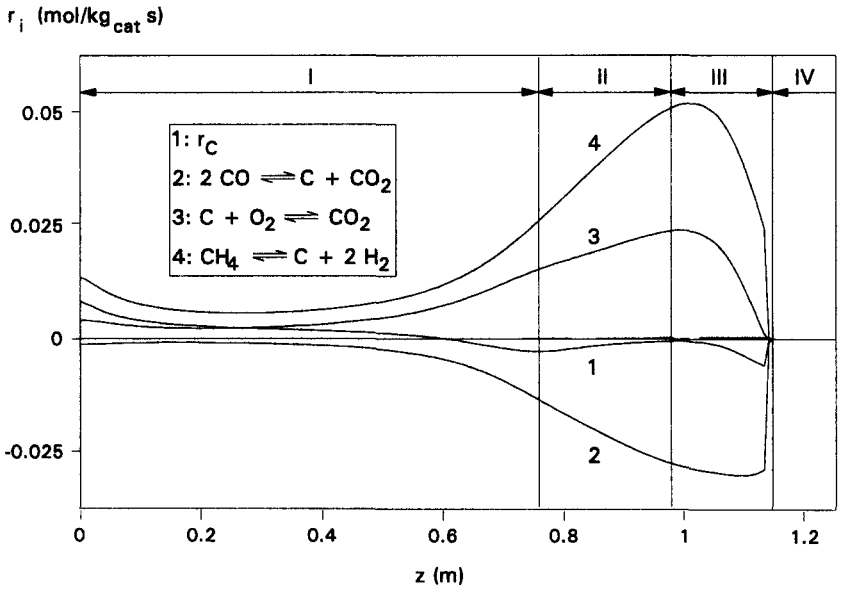

Fig. 4. Rate of carbon formation and carbon gasification through the catalyst bed after 5 min of reactor operation.

From a certain axial position onwards (zone II), the rate of carbon gasification by oxygen increases less rapidly because of the decreasing coke content of the catalyst.

From the corresponding temperature profile after 5 min of reactor operation in Fig. 2, it follows that the temperature starts to drop at an axial position of about 1 m (zone III). The heat effect of the endothermic methane cracking and of the reverse Boudouard reaction then exceeds that of the exothermic total combustion of methane and of the carbon gasification by oxygen. The lower temperature decreases the rate of methane cracking into coke

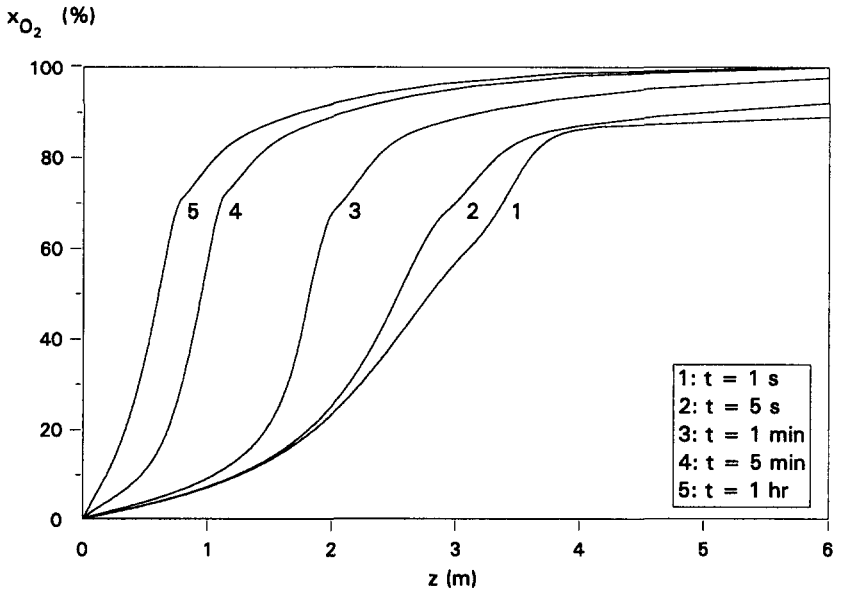

Fig. 5. Conversion of oxygen through the catalyst bed for several run lengths.

and of carbon gasification by oxygen. The rate of CO_2-gasification of carbon exhibits a maximum further downstream in the reactor. Indeed, the partial pressure of carbon dioxide increases due to the combustion of methane and the carbon gasification by oxygen and this has a more important influence on the reaction rate than the lower temperature. Because of the faster reverse Boudouard reaction the net gasification rate increases again. The temperature continues to decrease.

The carbon free zone of the reactor (zone IV) starts at an axial position of about 1.2 m. In this zone the heat effects of the various coking and gasification reactions which result in a net endothermic behaviour, do not occur anymore so that the temperature increases again from this position onwards. This explains the two humps in the temperature profiles in Fig. 2.

The decrease in the exit temperature with time is mainly due to the evolution of the rate of methane combustion and carbon gasification by oxygen. The molar heat of the total combustion of methane is higher than that of the gasification of coke by oxygen. Furthermore, the fraction of oxygen consumed in the carbon gasification reaction increases with time, so that less oxygen is available for the total combustion of methane into carbon dioxide and steam. Since the total oxygen conversion (Fig. 5) increases less rapidly with time than the fraction of oxygen consumed by carbon gasification, the overall process becomes less exothermic and leads to a lower exit temperature.

The outlet conversion of methane decreases with time, as is shown in Fig. 6. A significant fraction of the oxygen is consumed in the carbon gasification reaction, so that a smaller fraction of oxygen remains available for the total combustion of methane into carbon dioxide and steam. This is illustrated in Fig. 7, in which the rate of total combustion is shown for several run lengths (the surface area under the curves is a measure for the amount of methane consumed). The two humps in the rate curves correspond with the two humps in the temperature profiles. The amount of methane consumed in the steam reforming reaction increases with time (Fig. 8). This cannot compensate for the smaller amount of methane consumed in the total combustion reaction.

The evolution of the conversion of methane into CO for several run lengths is given in Fig. 9. The exit conversion into CO increases with time. The carbon gasification by oxygen becomes more and more important with the run length, thus leading to a higher CO_2-production. This in turn causes a higher consumption rate of CO_2 in the reverse Boudouard reaction, so that a higher conversion into CO is obtained.

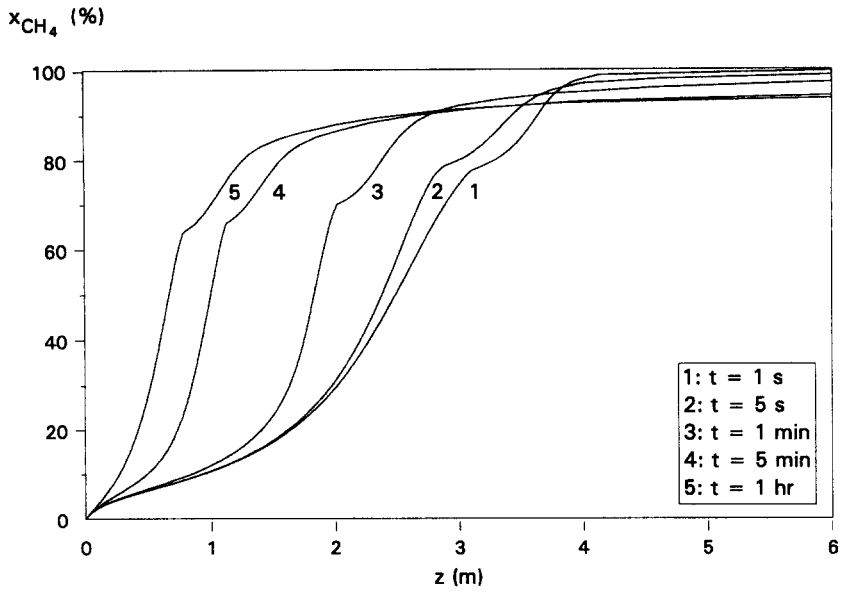

Fig. 6. Conversion of methane through the catalyst bed for several run lenghts.

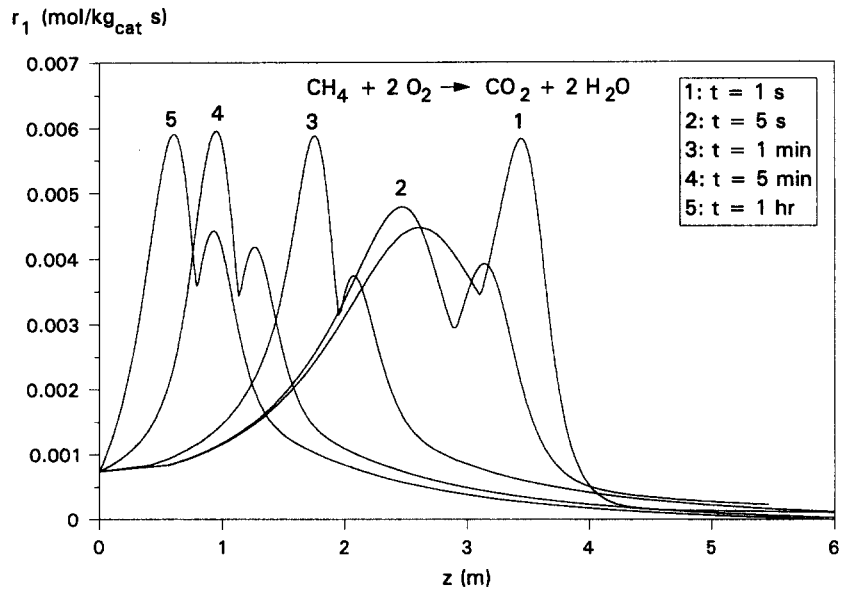

Fig. 7. Effective rate of the total combustion of methane into carbon dioxide and steam at several run lengths.

The zone of the reactor in which carbon is deposited, narrows with time, as can be seen in Fig. 10. Net coking only occurs in zone I of the reactor, as discussed earlier. From zone II onwards, gasification takes place. Because of the displacement of the reaction front towards the reactor inlet, zone I becomes shorter, so that the fraction of the catalyst bed covered with carbon shortens. After about 1 h of operation, the coke content of the catalyst hardly changes with time, and a steady state operation is reached. This is also illustrated in Table 2, in which the exit flow rates of H_2 and CO are given for various clock times. The ratio H_2/CO of the produced synthesis gas is also given.

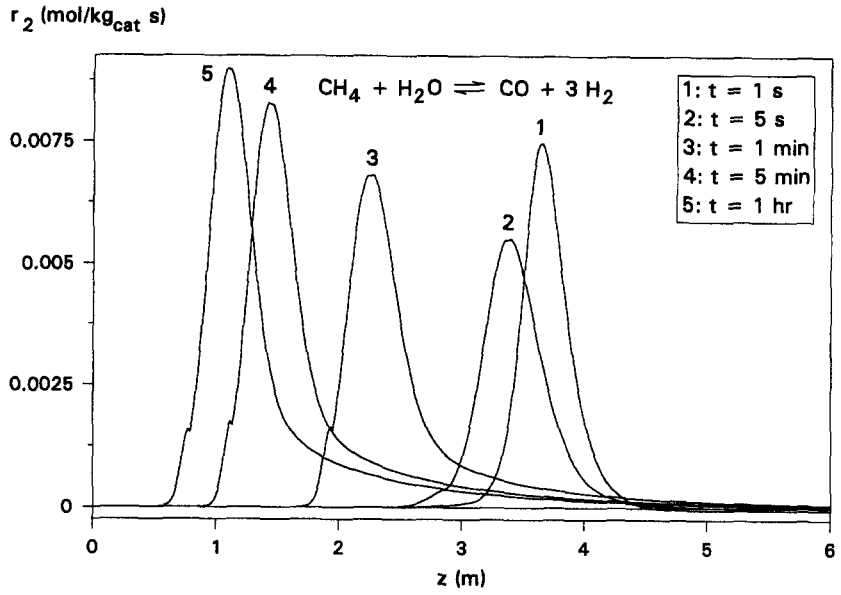

Fig. 8. Rate of CO-production by steam reforming through the catalyst bed for several run lengths.

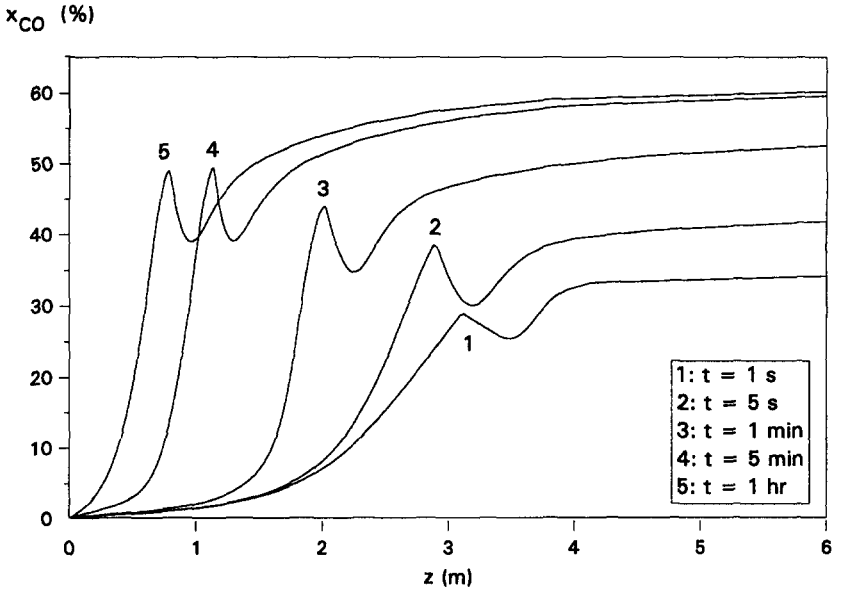

Fig. 9. Conversion of methane into carbon monoxide through the catalyst bed for several run lengths.

The exit conversions of CH_4 and O_2, the exit conversions of CH_4 into CO and CO_2, the effluent composition and the exit temperature after 1 h operation are given in Table 3.

The H_2/CO-ratio of the effluent, 3.2, is quite high. The choice of the feed conditions in this simulation was based upon the operating conditions of an industrial autothermal reformer [17]. Since steam was present in the feed, the H/C-feed ratio is higher and leads to a synthesis gas with higher H_2/CO-product ratio. The observed value was

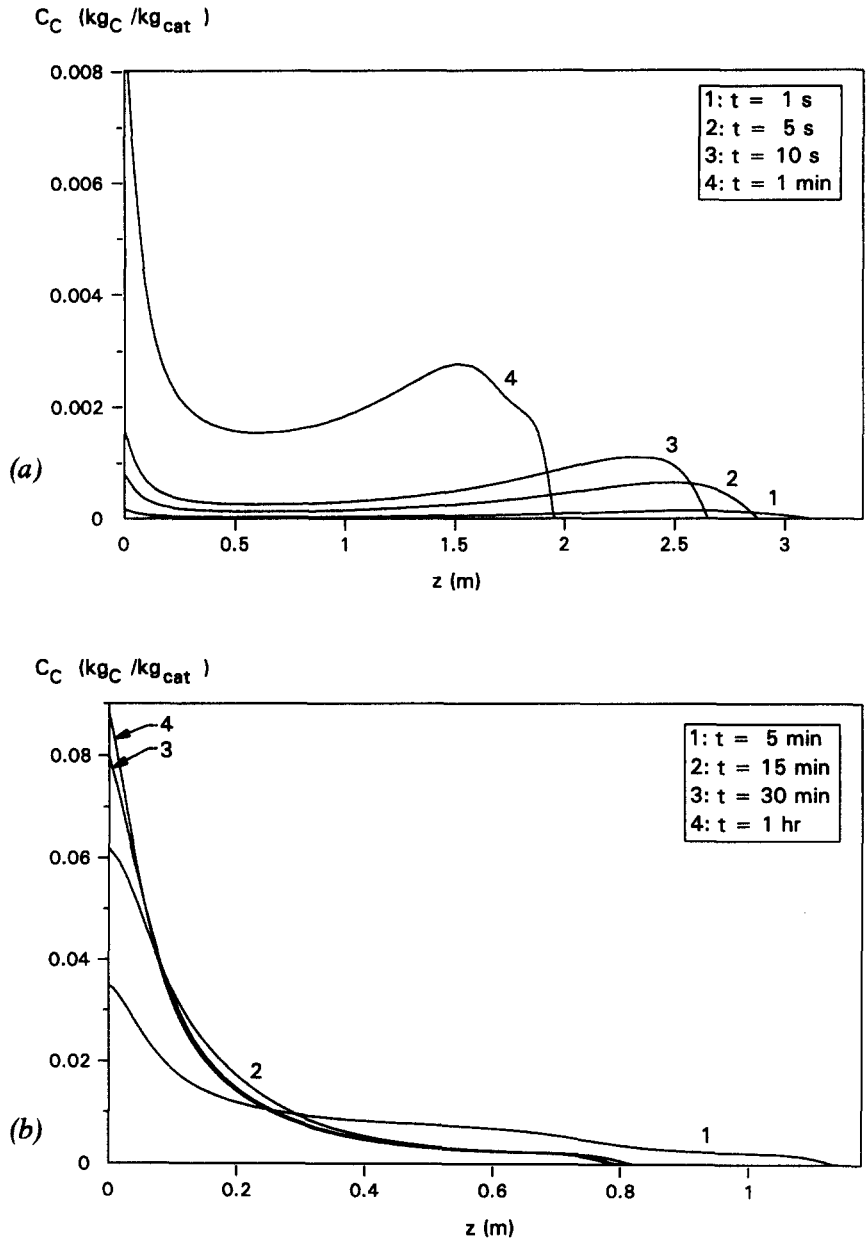

Fig. 10. Coke content of the catalyst during the first minute of operation (a) and for longer run lengths (b).

about 3. It also follows from the tables that the effluent still contains a small amount of methane, together with about 5% CO_2.

3.2. *Influence of the feed composition on the coke formation and coke content of the catalyst*

The influence of the addition of CO_2 and of steam on the coke deposition in the partial oxidation of methane with air or oxygen was also investigated. All simulations were performed with an inlet temperature of 808 K and an inlet

Table 2
Outlet conditions as a function of clock time

t (s)	$F_{t,out}$ (Nm^3/h)	$F_{H_2,out}$ (Nm^3/h)	$F_{CO,out}$ (Nm^3/h)	H_2/CO
1	19538	5950	1191	5.00
2	19648	6056	1257	4.82
5	19962	6129	1460	4.20
10	20282	6520	1680	3.88
60	20495	6642	1836	3.62
300	22819	6807	2083	3.27
900	22834	6813	2105	3.24
1800	22835	6814	2108	3.23
3600	22833	6813	2104	3.24

Table 3
Exit conditions and conversions after 1 h operation time

Exit temperature, T_{out} (K)	1140
Exit conversion of CH_4, x_{CH_4} (%)	93.64
Exit conversion of O_2, x_{O_2} (%)	100
Exit conversion into CO, x_{CO} (%)	60.09
Exit conversion into CO_2, x_{CO_2} (%)	33.40
Exit mole fraction of O_2, y_{O_2}	0
Exit mole fraction of N_2, y_{N_2}	0.3476
Exit mole fraction of CH_4, y_{CH_4}	0.0097
Exit mole fraction of H_2, y_{H_2}	0.2976
Exit mole fraction of CO, y_{CO}	0.0917
Exit mole fraction of CO_2, y_{CO_2}	0.0512
Exit mole fraction of H_2O, y_{H_2O}	0.2021

Table 4
Feed conditions for the partial oxidation of methane with air

	Feed 1	Feed 2	Feed 3	Feed 4
p_t^0 (atm)	25	25	25	25
T^0 (K)	808	808	808	808
F_t^0 (Nm^3/h)	18375	13498	20417	14998
H_2O/CH_4	1.4	0	1.4	0
CH_4/O_2	1.672	1.672	1.672	1.672
$y_{H_2}^0$	0.0001	0.0001	0.0001	0.0001
$y_{CO_2}^0$	0	0	0.1	0.1

total pressure of 25 atm. The inlet flow rate of methane was set at a constant value of 3500 Nm^3/h, so as to compare the quasi-steady state coke content of the catalyst (coke content after 1 h of operation).

3.2.1. *Partial oxidation with air*

The quasi-steady state coke content of the catalyst for the partial oxidation of methane with air is shown in Fig. 11. The corresponding feed conditions are given in Table 4. The exit conversions, exit temperature, H_2/CO-product ratio and effluent composition are presented in Table 5.

3.2.1.1. Influence of steam addition. When steam is added to the feed mixture, the coke content of the catalyst is higher and coke is deposited in a larger zone of the catalyst bed. This was already shown in the previous section,

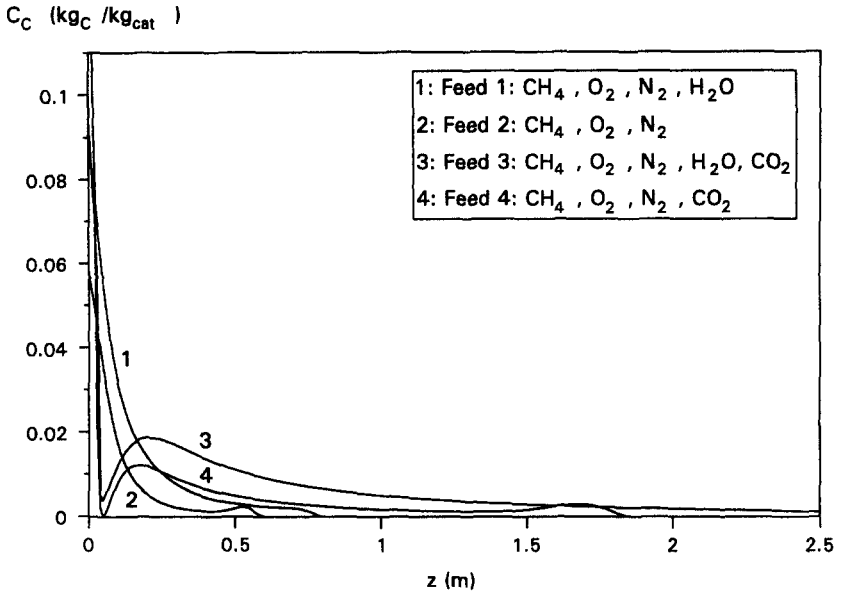

Fig. 11. Quasi-steady state coke content of the catalyst: Influence of the addition of CO_2 and H_2O.

where the rate of carbon gasification by steam was found to be negligible. Since the methane flow rate is kept constant, the addition of steam results in a lower partial pressure of oxygen, leading to a lower rate of carbon gasification by oxygen and a higher coke content of the catalyst. When no steam is added to the feed, a small peak is observed at the downstream end of the coke profile.

Fig. 12 shows the evolution of the carbon formation and gasification reactions for a feed without steam after 5 min of operation. The coking and gasification rates, and the net coking rate for the corresponding feed with steam were already shown in Fig. 4. As indicated before, the gasification rate increases continuously at the end of zone I, then starts to decrease and reaches a minimum at the end of zone II, though no coking occurs. When no steam is present in the feed, the net gasification rate decreases too, but changes into a net coking rate that reaches a maximum at the end of zone II, as is shown in Fig. 12. This leads to a maximum in the coke content of the catalyst at the corresponding axial position. The net coke formation is caused by the slower reverse Boudouard reaction. At an axial position of about 0.5 m the rate of CO-production by steam reforming becomes significant and CO is produced, thus inhibiting the production of CO by the reverse Boudouard reaction. The methane cracking reaction also slows down, due to the formation of H_2, but to a lesser extent since the partial pressure of methane is still high. Further downstream the reactor, the steam reforming reaction (2) reverses, since significant amounts of CO and H_2 are formed by the reverse Boudouard reaction and by methane cracking. There is again a net coke gasification. Because the reaction front moves towards the reactor inlet with time, the small peak at the end of the profile of the coke content of the catalyst will be located earlier in the catalyst bed during steady state operation.

The addition of steam to the feed is reflected in the exit temperature and in the product ratio of the syngas (Table 5). When steam is added, steam reforming starts earlier in the reactor. The maximum temperature is lower, and this slows down the reforming and combustion rates. The lower partial pressure of methane also contributes to this. Because of the presence of steam, the equilibrium in the WGS-reaction shifts towards CO_2 and H_2, thus explaining the higher conversion into CO_2 and the higher H_2/CO-ratio in the effluent.

3.2.1.2. Influence of the addition of carbon dioxide. When CO_2 is added to the feed, the coke content of the catalyst decreases faster in the first part of the reactor, passes through a minimum and then goes through a maximum (Fig. 11). The form of the coke profile behind the maximum depends upon the steam content. When

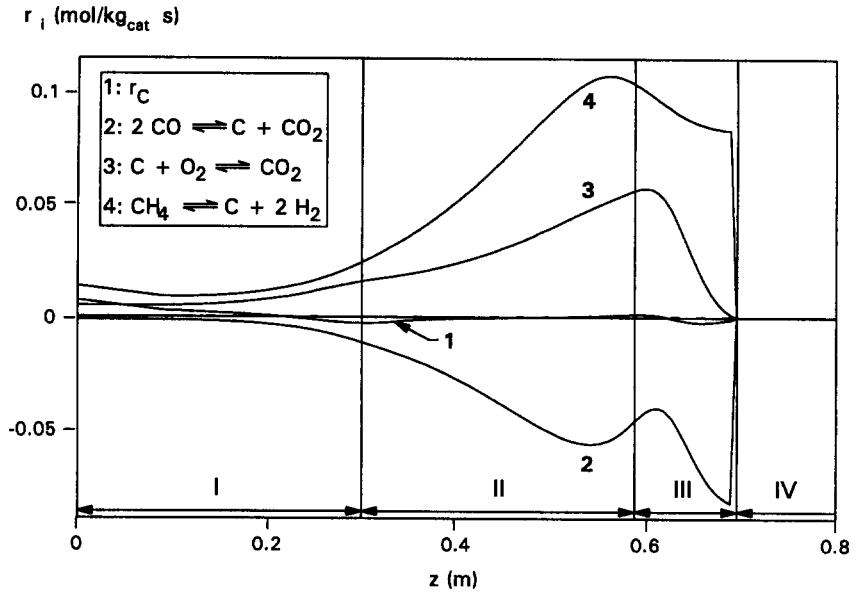

Fig. 12. Net coking rate r_C and rate of the carbon formation and gasification reactions for feed 2 (CH_4/air/H_2) after 5 min of reactor operation.

Table 5
Exit conditions for the partial oxidation of methane with air: Influence of the addition of steam and CO_2

	Feed 1	Feed 2	Feed 3	Feed 4
T_{out} (K)	1140	1218	1067	1133
$F_{t,out}$ (Nm^3/h)	22833	15249	22853	16867
F_{H_2} (Nm^3/h)	6813	4742	5133	3933
F_{CO} (Nm^3/h)	2104	2493	2301	3083
H_2/CO	3.24	1.90	2.23	1.28
x_{O_2} (%)	100	100	96.03	100
x_{CH_4} (%)	93.64	89.52	85.36	85.97
x_{CO} (%)	60.09	82.49	70.16	98.69
x_{CO_2} (%)	33.40	7.45	15.17	−12.59
y_{O_2}	0	0	0.0034	0
y_{N_2}	0.3476	0.4459	0.3230	0.4167
y_{CH_4}	0.0097	0.0208	0.0210	0.0260
y_{H_2}	0.2976	0.3110	0.2246	0.2332
y_{CO}	0.0917	0.1635	0.1007	0.1828
y_{CO_2}	0.0512	0.0148	0.1055	0.0559
y_{H_2O}	0.2021	0.0440	0.2216	0.0854

there is no CO_2 in the feed, the coke content of the catalyst continuously decreases. The rates of the major carbon production and gasification reactions, and the net coking rate after 5 min of reactor operation for a feed containing CO_2 are presented in Fig. 13. In the first part of the reactor the reverse Boudouard reaction rapidly accelerates, while the rate of methane cracking slowly decreases. Carbon gasification with oxygen slows down too, due to the lower coke content of the catalyst. This decrease is more than compensated for by the faster reverse Boudouard reaction, so that a minimum occurs in the coke profile.

Addition of carbon dioxide to the feed is mainly reflected in the H_2/CO-product ratio, as can be seen in Table 5. Adding CO_2 to the feed decreases the conversion of methane, but increases the conversion into CO, thus leading to a syngas with lower H_2/CO-ratio.

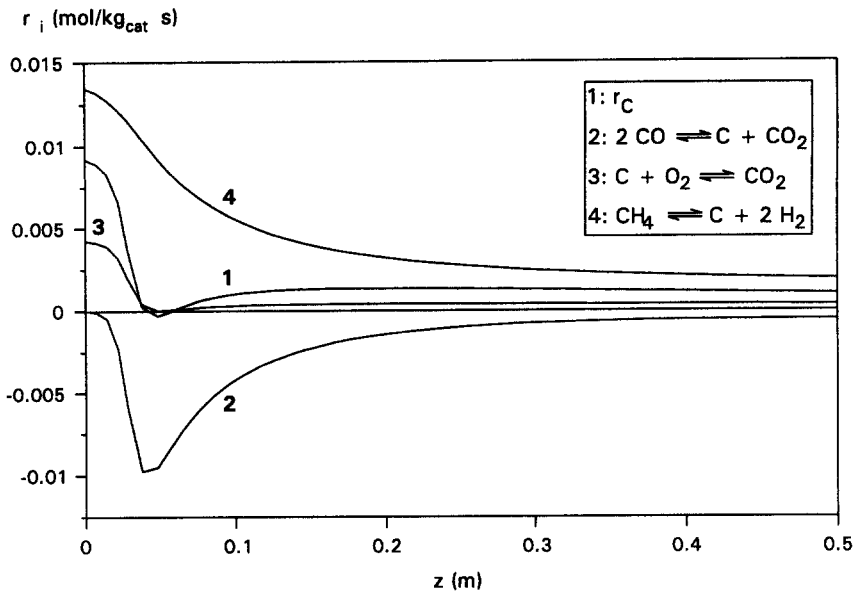

Fig. 13. Net coking rate r_C and rate of the carbon formation and gasification reactions for feed 4 (CH_4/air/CO_2/H_2) after 5 min of reactor operation.

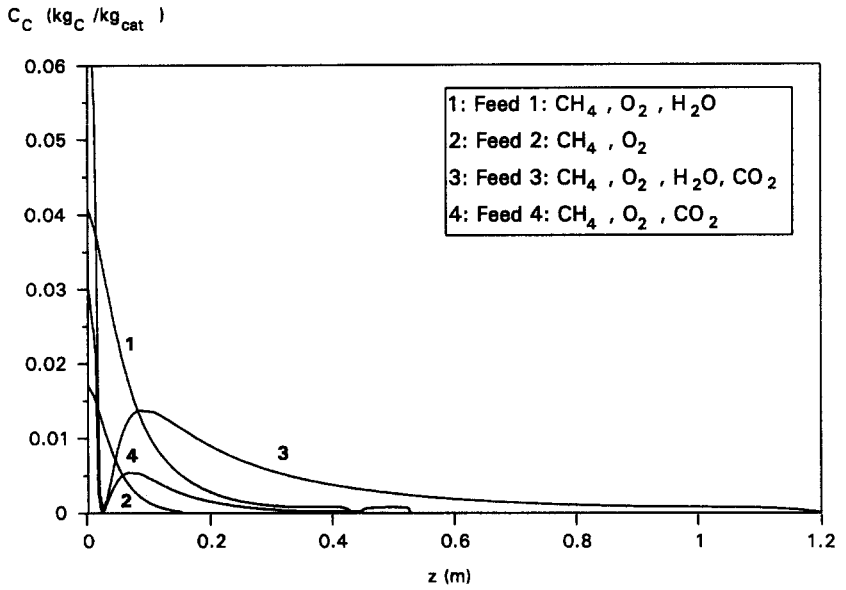

Fig. 14. Quasi-steady-state coke content of the catalyst in the partial oxidation of methane with oxygen. Influence of the addition of CO_2 and H_2O.

3.2.2. *Partial oxidation with oxygen*

The evolution of the coke content of the catalyst through the reactor during steady state operation for the partial oxidation of methane with oxygen is given in Fig. 14. The corresponding feed conditions are presented in Table 6. The form of the coke profiles is similar to that for the partial oxidation of methane with air. The amount of coke is lower because of the higher partial pressures of oxygen. The area in which coke is deposited is smaller than in the

Table 6
Feed conditions for the partial oxidation of methane with oxygen

	Feed 1	Feed 2	Feed 3	Feed 4
p_t^0 (atm)	25	25	25	25
T^0 (K)	808	808	808	808
F_t^0 (N m^3/h)	10490	5584	11661	6184
H_2O/CH_4	1.4	0	1.4	0
CH_4/O_2	1.672	1.672	1.672	1.672
$y^0_{H_2}$	0.0001	0.0001	0.0001	0.0001
$y^0_{CO_2}$	0	0	0.1	0.1

Table 7
Partial oxidation of methane with air: Influence of the CH_4/O_2-feed ratio on exit values

	CH_4/O_2=1	CH_4/O_2= .672	CH_4/O_2=2	CH_4/O_2=3
T_{out} (K)	1418	1219	1170	1109
$F_{t,out}$ (Nm^3/h)	21654	15236	13287	9780
F_{H_2} (Nm^3/h)	4673	4752	6936	3354
F_{CO} (Nm^3/h)	2746	2479	1972	981
H_2/CO	1.70	1.92	2.16	3.42
x_{O_2} (%)	80.20	100	100	100
x_{CH_4} (%)	99.92	89.93	80.96	67.88
x_{CO} (%)	88.15	82.11	65.53	33.34
x_{CO_2} (%)	11.22	7.47	6.98	5.77
W_C (kg$_C$)	397	347	14511	44412

case of partial oxidation with air, too. This could be expected, since the temperature peak is shifted towards the reactor inlet when oxygen is used instead of air.

3.3. *Influence of the operating conditions*

The influence of the inlet temperature, the total pressure and the CH_4/O_2-feed ratio on the coke deposition in the partial oxidation of methane with air was also investigated. The base case has an inlet temperature of 808 K, a total pressure of 25 atm and a CH_4/O_2-feed ratio of 1.6722. Again the feed flow rate of methane is 3500 Nm^3/h in all cases, so as to compare the quasi-steady state coke content of the catalyst.

3.3.1. *Influence of the CH_4/O_2-feed ratio*

Simulations are performed for the partial oxidation of CH_4/air-mixtures with methane/oxygen-ratios of 1, 1.6722, 2 and 3. Since the feed flow rate of methane is kept constant in all simulations, a variation of the CH_4/O_2-ratio implies a change in the total feed flow rate.

The total inlet and exit flow rate, the exit temperature, the flow rates of CO and H_2 at the exit, the H_2/CO-ratio of the synthesis gas and the total amount of coke deposited in the reactor after 1 h of operation, W_C, are given in Table 7. The profile of the coke content of the catalyst after a run length of 1 h is shown in Fig. 15.

It follows from Table 7 that the coke content of the catalyst is at a minimum for a feed ratio of 1.6722. The minimum coke content corresponds with the highest selectivity for CO. The table also shows that partial oxidation of feed mixtures with high CH_4/O_2-ratio (>2) is not feasible, due to severe coke formation.

The existence of an optimal CH_4/O_2-feed ratio can be explained as follows. For feeds with low CH_4/O_2-feed ratio a larger amount of methane is consumed in the total combustion reaction when the feed ratio is increased. This leads to a steeper temperature profile and a higher temperature in the first part of the catalyst bed. The methane cracking

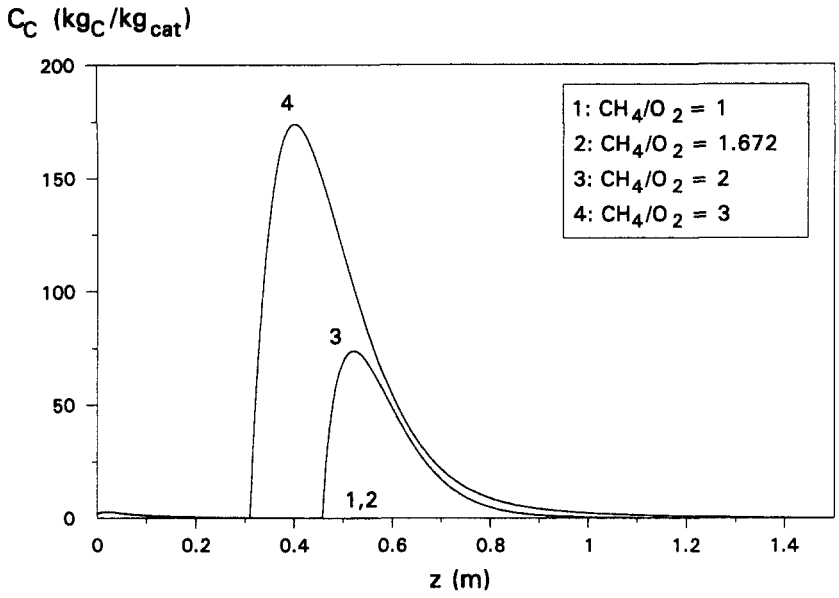

Fig. 15. Evolution of the coke content of the catalyst after 1 h of operation: Influence of the CH_4/O_2-feed ratio.

Table 8
Partial oxidation of methane with air: Influence of the total pressure on exit values

	p=10 atm	p=25 atm	p=50 atm
T_{out} (K)	1161	1219	1254
$F_{t,out}$ (Nm^3/h)	15373	15236	15245
F_{H_2} (Nm^3/h)	5126	4752	4374
F_{CO} (Nm^3/h)	2609	2479	2499
H_2/CO	1.96	1.92	1.75
x_{O_2} (%)	100	100	100
x_{CH_4} (%)	94.78	89.93	82.77
x_{CO} (%)	87.27	82.11	81.42
x_{CO_2} (%)	7.06	7.47	7.57
W_C	1007	347	145

and the gasification of coke by oxygen are thus promoted, but the carbon gasification by oxygen is accelerated more rapidly, leading to a lower coke content of the catalyst.

For oxygen deficient methane/air-mixtures, all the oxygen is consumed in the first part of the reactor and a considerable amount of methane remains unreacted. Together with the relatively high temperature this favours methane cracking so that more coke is deposited and in a larger zone of the catalyst bed (Fig. 15). The higher rate of methane cracking also explains the high H_2/CO-product ratio of the produced syngas. Since oxygen is consumed both in the total combustion of methane and in the gasification of coke by oxygen, the optimal CH_4/O_2-feed ratio lies between 1.7 and 1.8.

3.3.2. *Influence of the total pressure*

The total pressure at the reactor inlet was varied between 10 and 50 atm. The simulation results are compared in Table 8. The evolution of the coke content of the catalyst through the reactor for a run length of 1 h is presented in Fig. 16.

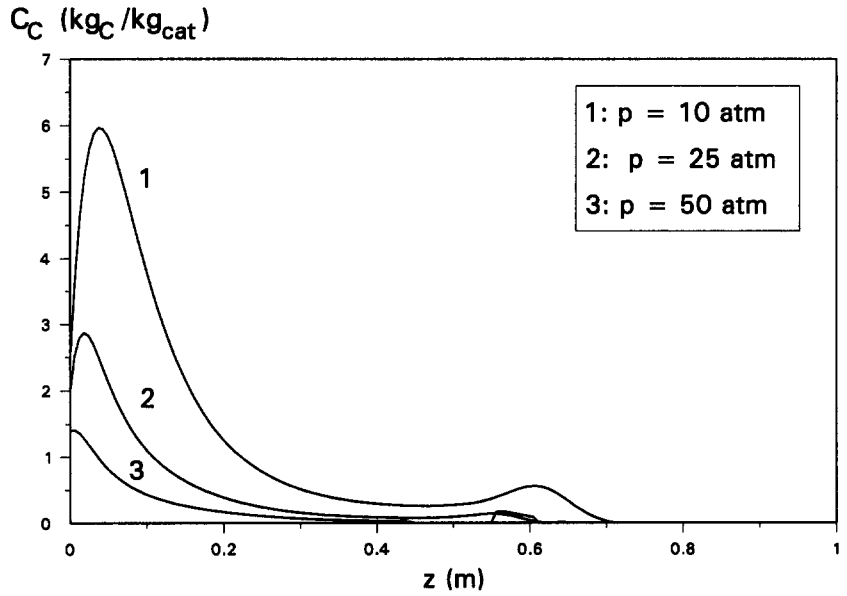

Fig. 16. Coke content of the catalyst after 1 h of operation: Influence of the total pressure at the inlet.

Table 9
Partial oxidation of methane with air: Influence of the inlet temperature on exit values

	T^0=658 K	T^0=708 K	T^0=808 K	T^0=858 K
T_{out} (K)	740	1190	1219	1236
$F_{t,out}$ (Nm^3/h)	13504	15130	15236	15288
F_{H_2} (Nm^3/h)	131	4531	4752	4857
F_{CO} (Nm^3/h)	9	2345	2479	2546
H_2/CO	14.47	1.93	1.92	1.91
x_{O_2} (%)	5.85	100	100	100
x_{CH_4} (%)	3.44	86.92	89.93	91.34
x_{CO} (%)	0.26	77.17	82.11	84.54
x_{CO_2} (%)	1.78	8.86	7.47	6.81
W_C	2151	2854	347	124

The conversion of methane and the H_2/CO-ratio of the synthesis gas decrease with increasing pressure. Operating at high pressures lowers the total amount of coke deposited on the catalyst surface significantly and enhances the selectivity towards CO. From Fig. 16 it also follows that the zone of the reactor where carbon is deposited is shortened.

Operating the reactor at high pressure also implies a high partial pressure of oxygen. This leads to a faster combustion of methane, but also to a higher rate of coke gasification by oxygen. Methane cracking is accelerated too, but to a lesser extent. Because of the higher combustion rates more CO_2 is produced, so that the rate of the reverse Boudouard reaction increases significantly. This also explains the lower H_2/CO-ratio of the syngas at high pressure.

3.3.3. *Influence of the feed temperature*

Simulations are performed for the partial oxidation of methane with air for inlet temperatures of 658, 708, 808 and 858 K. The total flow rate, the flow rate of CO and H_2, the conversions, the temperature and the H_2/CO-ratio at

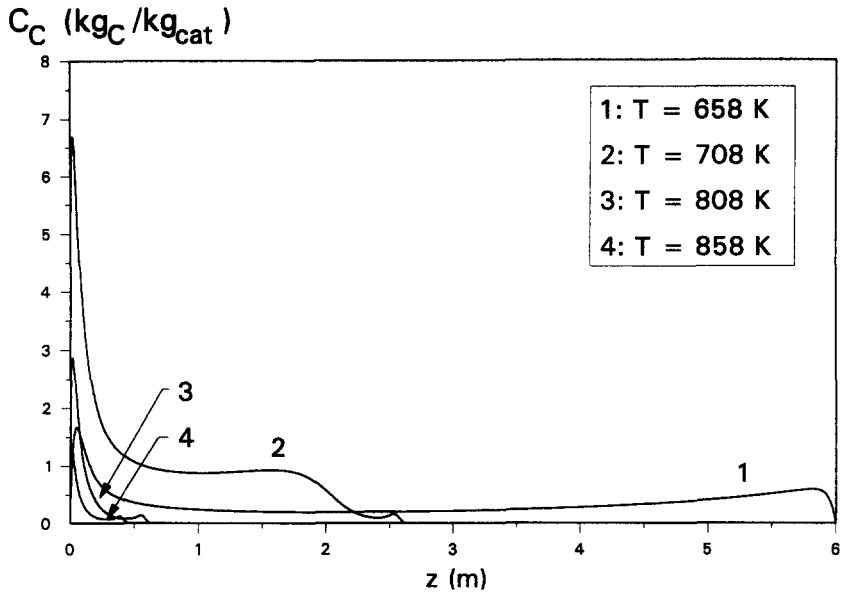

Fig. 17. Coke content of the catalyst after 1 h of operation: Influence of the feed temperature.

the reactor exit are given in Table 9. The total amount of coke deposited in the catalyst bed for a run length of 1 h is also shown. The coke profiles through the catalyst bed are presented in Fig. 17.

For temperatures leading to complete oxygen conversion, the H_2/CO-ratio of the synthesis gas remains practically constant. The conversion of methane and the selectivity to H_2 and CO slightly increase with temperature, so that more syngas is produced. The total carbon content of the catalyst decreases considerably for higher feed temperatures. The length of the zone of the reactor in which coke is deposited also shortens (Fig. 17).

For an inlet temperature of 658 K, coke is deposited over the whole reactor, since the rate of carbon gasification by oxygen at these low temperatures is not sufficiently high to gasify a significant fraction of the coke produced by methane cracking. The reverse Boudouard reaction only occurs near the end of the catalyst bed and is very slow too. At temperatures which allow complete conversion of oxygen, the amount of deposited coke decreases while the coking zone in the reactor shortens. Because of the higher temperature, the main partial oxidation reactions take place further upstream in the reactor and all reactions are accelerated. As already mentioned, the rate of methane cracking is less influenced by the temperature than the rates of the reverse Boudouard reaction and the coke gasification by oxygen. Therefore, the total weight of carbon in the catalyst bed after 1 h of reactor operation is decreased.

4. Conclusion

A stable reactor operation is possible for the partial oxidation of methane with air or oxygen, provided that appropriate operating conditions are chosen, even when small amounts of carbon are deposited on the catalyst surface. When air is used, methane conversions of 85% and higher are reached, depending upon the feed composition. The oxygen conversion varies between 96% and 100%. When oxygen is used instead of air, the methane conversion lies between 90% and 100%. The oxygen conversion is about the same. The coke content of the catalyst is lower and the zone in which carbon deposition occurs is shorter when oxygen is used instead of air.

The addition of carbon dioxide and/or steam leads to a significant change in the H_2/CO-ratio of the effluent. The addition of CO_2 increases the C/O- and C/H-ratio of the feed, thus leading to a syngas with low H_2-content. In the presence of steam the C/H-feed ratio is decreased and a synthesis gas with higher H_2/CO-ratio is processed. Changes in the feed composition are reflected in the quasi-steady state coke content of the catalyst as well. When steam is added, the coke content of the catalyst is higher and coke deposition occurs in a larger fraction of the reactor. This is in contradiction with the predictions in previous work, based upon a rate equation for carbon gasification by oxygen that is independent of the coke content of the catalyst. When carbon dioxide is added, the coke content of the catalyst decreases faster in the first part of the reactor because of the very rapid reverse Boudouard reaction.

Coke formation can also be reduced by operating at higher inlet temperatures and pressures. An optimal CH_4/O_2-feed ratio slightly lower than 2 was reached.

Symbols

C_C	coke content of the catalyst (kg_C/kg_{cat})
c_p	specific heat of fluid (kJ/kg K)
D_i	reactor diameter (m)
d_p	particle diameter (m)
f	friction factor in Fanning equation
F^0, F_t^0	total molar feed rate (kmol/h)
F_A^0	molar feed rate of reactant A (kmol/h)
F_A	flow rate of component A (Nm^3/h)
F_t	total molar flow rate ($kmol/m_r^2$ s)
$F_{t,out}$	total flow rate at the exit (Nm^3/h)
k_i	reaction rate constant
K_i	adsorption and equilibrium constants
L	reactor length (m)
p_A	partial pressure of component A (bar)
p_t, p_t^0	total pressure (bar)
r_1	reaction rate of total combustion ($kmol/m^3$ s)
r_2	reaction rate of CO-production by steam reforming ($kmol/m^3$ s)
r_3	reaction rate of CO_2-production by steam reforming ($kmol/m^3$ s)
r_4	rate of WGS-reaction ($kmol/m^3$ s)
r_5	rate of methane cracking ($kmol/m^3$ s)
r_6	rate of Boudouard reaction ($kmol/m^3$s)
r_7	rate of carbon gasification by steam ($kmol/m^3$ s)
r_8	rate of carbon gasification by oxygen ($kmol/m^3$ s)
r_C	net coking rate ($kmol/m^3$ s)
T, T^0	temperature (K)
T_{out}	temperature at the exit (K)
u_s	superficial velocity m_g^3/m_r^2 s
W_C	total amount of coke (kg_C)
x_{CH_4}	conversion of methane (%)
x_{CO}	conversion of methane into CO (%)
x_{CO_2}	conversion of methane into CO_2 (%)
x_{O_2}	conversion of oxygen (%)
y_A^0	mole fraction of component A in the feed
y_A	mole fraction of component A
z	axial position (m)

Greek symbols

η_1	effectiveness factor for total combustion
η_2	effectiveness factor for CO-production by steam reforming
η_3	effectiveness factor for CO_2-production by steam reforming
η_4	effectiveness factor for the WGS-reaction
η_5	effectiveness factor for methane cracking
η_6	effectiveness factor for the Boudouard reaction
η_7	effectiveness factor for carbon gasification by steam
η_8	effectiveness factor for carbon gasification by oxygen
ρ_b	catalyst bulk density kg_{cat}/m_r^3
ρ_g	gas density kg/m_r^3
Ω	cross-section of reactor (m^2)

Acknowledgements

The authors are grateful to NFWO-Belgium for partial funding of this project. This work was originally presented at the 9th International Symposium on Large Chemical Plants, held in Antwerp, Belgium, 6–8 October 1995.

References

[1] M.V. Twigg, Catalyst Handbook, 2nd ed., Wolfe Publishing, London, 1989.
[2] M. Prettre, Ch. Eichner and M. Perrin, Trans. Faraday Soc., 23 (1946) 335–340.
[3] P.D.F. Vernon, M.L.H. Green, A.K. Cheetham and A.T. Ashcroft, Catal. Today, 13 (1992) 417–426.
[4] C.F. Cullis, D.E. Keene and D.L. Trimm, J. Catal., 19 (1970) 378–385.
[5] D.L. Trimm and C.-W. Lam, Chem. Eng. Sci., 35 (1980) 1405–1413.
[6] J. Xu and G.F. Froment, A.I.Ch.E. J., 35 (1989) 88–96.
[7] M.A. Soliman, S.S.E.H. El-Nashaie, A.S. Al-Ubaid and A. Adris, Chem. Eng. Sc., 43 (1988) 1801–1806.
[8] D. Dissanayake, M.P. Rosynek, K.C.C. Kharas and J.H. Lunsford, J. Catal., 132 (1991) 117–127.
[9] E.S. Wagner, G.F. Froment, 1990, unpublished results.
[10] J.-W. Snoeck, G.F. Froment, 1995, to be published.
[11] A.M. De Groote and G.F. Froment, Rev. Chem. Eng., 11 (1995) 145–183.
[12] A.M. De Groote and G.F. Froment, Appl. Catal. A, 138 (1995) 245–264.
[13] P.B. Weisz and R.B. Goodwin, J. Catal., 6 (1966) 227–236.
[14] G.F. Froment, K.B. Bischoff, Chemical Reactor Analysis and Design, 2nd ed., Wiley, New York, NY, 1990.
[15] J. Xu and G.F. Froment, A.I.Ch.E. J., 35 (1989) 97–102.
[16] H.P. Press, B.P. Flannery, S.A. Teukolsky, W.T. Vetterling, Numerical Recipes, 3rd ed., Cambridge University Press, Cambridge, 1988.
[17] A. Lowson, I. Primdahl, D. Smith, S. Wang, Proceedings of the A.I.Ch.E. Spring National Meeting, 1990.